PHYSICAL REVIEW B VOLUME 29, NUMBER 2 15 JANUARY 1984

Local-environment fluctuations and densities of states in substitutionally disordered alloys

A. Gonis
Department of Physics and Astronomy, Northwestern University, Evanston, Illinois 60201

G. M. Stocks and W. H. Butler
Metals and Ceramics Division, Oak Ridge National Laboratory, Oak Ridge, Tennessee 37830

H. Winter
Kernforschungszentrum Karlsruhe, D-7500 Karlsruhe, Federal Republic of Germany
(Received 8 June 1983)

We report calculations of densities of states (DOS) associated with specific atomic configurations of compact clusters in substitutionally disordered alloys describable by a Hamiltonian with nonoverlapping muffin-tin potentials. The method of calculation consists in evaluating the Green function associated with a cluster of atoms embedded in a translationally invariant effective medium such as the one determined in the Korringa-Kohn-Rostoker, coherent-potential-approximation (KKR-CPA) method. This method yields well-defined, analytic, and physically meaningful results and takes proper account of the crystal structure of the lattice. Numerical results are reported for near-neighbor clusters in both one-dimensional model muffin-tin alloys, as well as in realistic Ag_cPd_{1-c} alloys. The DOS associated with many cluster configurations exhibit more structure than the DOS calculated in the single-site KKR-CPA method, which can be understood in terms of fundamental physical quantities, such as the relative scattering strength of the alloy constituents, and of the symmetry of the lattice. Several possible applications of cluster DOS in calculating the physical properties of substitutionally disordered alloys are discussed.

I. INTRODUCTION

The coherent-potential approximation[1] (CPA) is the most satisfactory single-site theory for the discussion of the one-particle properties of random, substitutionally disordered alloys. In the CPA, one considers the real disordered material replaced with an effective medium that possesses the symmetry of the underlying lattice. Each site of the lattice is occupied by an effective scatterer determined through the self-consistency condition that the scattering off a real atom embedded in the medium vanishes on the average. The CPA has many desirable properties, and has been reviewed extensively in the literature.[2,3] It has also been used successfully to calculate electronic densities of states[4,5] (DOS's) and transport properties[6,7] of disordered substitutional alloys.

In spite of its many desirable properties, however, the CPA, as a single-site theory, cannot account for the effects of fluctuations in the local environment of a site. Such fluctuations are responsible for sharp structure in the DOS and may strongly influence physical properties, e.g., the formation of magnetic moments. In addition, short-range order (SRO) can only be taken into account accurately and convincingly within the context of a multisite, rather than a single-site, theory.

The need to extend the ideas embodied in the CPA to a cluster theory was realized almost simultaneously with the introduction of the CPA, and several attempts have been reported[8–21] toward such an extension. These attempts produced theories that were either too difficult to implement computationally, such as the molecular CPA,[19] or were shown[20] to lack analytical rigor. In other applications,[21] severe simplifications such as the substitution of a Cayley-tree (or Bethe) lattice for the proper crystal structure of the material surrounding the cluster were made.

The original applications of the CPA as well as all attempts toward cluster generalizations were made in connection with tight-binding (TB) or interpolation-scheme Hamiltonians. The first satisfactory cluster method was consequently developed[22] with respect to such Hamiltonians. This method, which strikes a balance between conceptual simplicity, analytical rigor, and computational ease, has been used in several applications[22,23] in connection with model electron and phonon systems. In this method, one solves for the Green's function (or scattering matrix) for a cluster of real atoms embedded in an effective medium which is determined within the single-site CPA. The advantages as well as the limitations of this method have been discussed in a previous publication.[22]

TB Hamiltonians are relatively easy to handle computationally and are appropriate for many applications, but also possess severe limitations with respect to a wide class of disordered systems. One important limitation is the need for parametrization procedures in order to determine the values of the various physical quantities that enter a calculation. For alloys of constituents with different bandwidths, for example, a TB description requires the introduction of off-diagonal disorder (ODD), i.e., disorder in the site off-diagonal elements of the TB Hamiltonian as well as in the diagonal ones. The parameters that describe ODD can be determined only by means of oversimplified interpolation schemes. Such limitations can be removed

within the context of a Hamiltonian with nonoverlapping muffin-tin (MT) potentials.

The application of the CPA to systems described by MT Hamiltonians is a much more arduous computational task than the application to TB systems and, therefore, it has materialized comparatively slowly. Now, however, the computational tools for applying the CPA to MT Hamiltonians have been developed.[3,24] These computational techniques are similar[25,26] to those used in Korringa-Kohn-Rostoker (KKR) calculations of DOS in pure metals, and an extensive review of these techniques has appeared in a recent publication.[25] It is now generally acknowledged that the KKR-CPA method provides a reliable, first-principles description of band structure and related electronic properties of disordered substitutional alloys.

In this paper, we extend the cluster method originally developed[22] in connection with TB Hamiltonians to alloys describable by MT Hamiltonians. We apply the method to a cluster consisting of a central site and its shell of nearest neighbors embedded in a medium determined within the KKR-CPA method. The DOS's are obtained from the site-diagonal element of the Green's function at the center of the cluster, calculated using a cluster generalization of the KKR-CPA formulas. Thus these are the first *a priori* cluster DOS calculations based on the actual potential functions of an alloy and taking realistic account of local-environment effects and of the proper crystal structure of the material. An independent and different derivation of our formulas has recently appeared[27] in a treatment of a cluster of impurity atoms embedded in a pure host.

The rest of the paper is arranged as follows. In Sec. II we briefly rederive the KKR-CPA self-consistency condition in a form that lends itself naturally to the cluster generalization presented in Sec. III. This form also brings out the similarity of the cluster method as applied to TB and MT systems. In Sec. IV we describe the method used to evaluate the off-diagonal elements of the cluster Green's function. Section V contains the results of numerical applications of the cluster method to a one-dimensional model MT alloy as well as to Ag_cPd_{1-c} alloys. A summary and a discussion of the method and its potential applications are contained in Sec. VI.

II. REDERIVATION OF THE KKR-CPA

The KKR-CPA method has been discussed[3,24,25] extensively in the literature. In this section, we present a condensed derivation of the self-consistency condition of the KKR-CPA method in a form that allows the straightforward generalization to the cluster method presented in the following section.

The electronic Hamiltonian of the substitutionally disordered MT alloy is taken to be of the form

$$H=-\nabla^2+V\ , \tag{2.1}$$

where the potential function V corresponds to a collection of nonoverlapping MT potentials,

$$V(r)=\sum_n v(\vec{r}-\vec{R}_n)=\sum_n v(\vec{r}_n)\ . \tag{2.2}$$

Here, $v(\vec{r}-\vec{R}_n)$ is the potential centered on site n and is assumed to vanish outside S_n, the radius of the MT sphere centered at $\vec{R}_n$. In a random substitutional binary alloy, A_cB_{1-c}, $v(\vec{r}_n)$ can assume the values $v^A(r_n)$ or $v^B(r_n)$, with corresponding probabilities c and $1-c$, respectively.

The single-particle properties of the alloy are given by the ensemble average $\langle G\rangle$ of the one-particle Green's-function operator. For any alloy configuration and for a given energy ϵ, the Green's function is given by the expression[24]

$$G(\epsilon;\vec{r},\vec{r}')=\sum_{LL'} Z_L^n(\epsilon,\vec{r}_n)\tau_{LL'}^{nm}Z_{L'}^m(\epsilon,\vec{r}'_m) - \sum_L Z_L^n(\epsilon,\vec{r}_n)J_L^n(\epsilon,\vec{r}_n)\delta_{nm}\ . \tag{2.3}$$

In this expression, $\vec{r}(\vec{r}')$ is within the cell centered at $\vec{R}_n(\vec{R}_m)$. The $Z_L^n(\epsilon,\vec{r}_n)$ and $J_L^n(\epsilon,\vec{r}_n)$ are solutions of the Schrödinger equation for a single MT potential $v(\vec{r}_n)$ corresponding to angular momentum indices $L(=l,\mu)$. $Z_L^n(\epsilon,\vec{r}_n)$ is regular at the origin and joins smoothly to the function

$$Z_L^n(\epsilon,\vec{r}_n)=[j_l(\kappa r)m_L^n-i\kappa h_l(\kappa r)]Y_L(\hat{r})\ , \tag{2.4}$$

at $r_n=S_n$. Here, j_l and h_l denote the spherical Bessel and Hankel functions and $\kappa=\sqrt{\epsilon}$. $J_L^n(\epsilon,\vec{r}_n)$ joins smoothly to $j_l(\kappa r_n)Y_L(\vec{r}_n)$ at $r_n=S_n$ and is not regular at the origin in general. The $\tau_{LL'}^{nm}(\epsilon)$ are the on-the-energy-shell matrix elements of the scattering path operator defined by Gyorffy and Stott,[26] and are given by the inverse of the matrix $\underline{M}$,

$$\tau_{LL'}^{nm}=[\underline{M}^{-1}]_{LL'}^{nm}\ , \tag{2.5}$$

$$M_{LL'}^{nm}=m_{LL'}^n\delta_{nm}\delta_{LL'}-g_{LL'}^{nm}\ . \tag{2.6}$$

In these equations, m^n is the inverse of the site-diagonal t matrix, $m^n=t_n^{-1}$, which for a spherical MT potential is diagonal in the angular momentum indices. The $g_{LL'}^{nm}$ are the elements of the free-electron Green's function. For a complete discussion of the form taken by the averaged Green's function and for the expressions for calculating DOS in the CPA, the reader is directed to Refs. 24 and 25.

It is clear from Eq. (2.3) that in order to evaluate the average of the site-diagonal element of the Green's function, one must evaluate the average of the corresponding element of the scattering path operator. The general matrix elements of this operator satisfy the equation of motion,

$$\tau_{LL'}^{nm}=t_L^n\left[\delta_{nm}\delta_{LL'}+\sum_{\substack{k\ (\neq n),\\ L''}} g_{LL''}^{nk}\tau_{L''L'}^{km}\right]\ , \tag{2.7}$$

or

$$\underline{\tau}^{nm}=\underline{t}^n\left[\delta_{nm}+\sum_{k\ (\neq n)}\underline{g}^{nk}\underline{\tau}^{km}\right]\ . \tag{2.8}$$

In Eq. (2.8) we suppress the angular momentum indices in order to simplify our notation. From Eq. (2.8) we obtain the equations

$$\underline{\tau}^{nn}=\underline{t}^{n}\left[1+\sum_{k\,(\neq n)}\underline{g}^{nk}\underline{\tau}^{kn}\right], \tag{2.9}$$

for the diagonal part, and

$$\underline{\tau}^{kn}=\underline{t}^{k}\underline{g}^{kn}\underline{t}^{nn}+\underline{t}^{k}\sum_{k\,(\neq n)}\sum_{l\,(\neq k,n)}\underline{g}^{kl}\underline{\tau}^{ln}, \tag{2.10}$$

for $k\neq n$.

Equation (2.10) can now be iterated with the second term on the right-hand side treated formally as a perturbation. When the resulting expression for $\underline{\tau}^{kn}$, in terms of $\underline{\tau}^{nn}$, is substituted into Eq. (2.9), one can express $\underline{\tau}^{nn}$ in the form

$$\underline{\tau}^{nn}=(\underline{m}^{n}-\underline{\Delta}^{n})^{-1}, \tag{2.11}$$

where the "renormalized interactor" $\underline{\Delta}^{n}$ has the real-space expansion,

$$\underline{\Delta}^{n}=\sum_{k\,(\neq n)}\underline{g}^{nk}\underline{m}^{k}\underline{g}^{kn}+\sum_{k\,(\neq n)}\sum_{l\,(\neq k,n)}\underline{g}^{nk}\underline{m}^{k}\underline{g}^{kl}\underline{m}^{l}\underline{g}^{ln}+\cdots . \tag{2.12}$$

It is clear from this expansion that $\underline{\Delta}^{n}$ represents the sum of all paths through the disordered material that start at site n and end at site n but avoid site n at all intermediate steps. It is also clear that $\underline{\Delta}^{n}$ depends on the constitution of the material surrounding site n but is independent of the potential on site n. If the disordered material is replaced by an effective medium characterized by a single-site effective scattering matrix $\underline{\bar{t}}$ (with $\underline{\bar{m}}=\underline{\bar{t}}^{-1}$) and a scattering path operator $\underline{\bar{\tau}}$, then Eq. (2.11) immediately yields the expressions

$$\underline{\Delta}^{n}=\underline{\bar{m}}-(\underline{\bar{\tau}}^{nn})^{-1} \tag{2.13}$$

and

$$\underline{\tau}^{nn}=[\underline{m}^{n}-\underline{\bar{m}}+(\underline{\bar{\tau}}^{nn})^{-1}]^{-1}. \tag{2.14}$$

The site-diagonal part of the effective-medium scattering path operator $\underline{\bar{\tau}}^{nn}$ is given by means of the Brillouin-zone (BZ) integral

$$\underline{\bar{\tau}}^{nn}=\frac{1}{\Omega_{\mathrm{BZ}}}\int_{\mathrm{BZ}}[\underline{\bar{m}}-\underline{g}(\vec{k})]^{-1}d^{3}k=\frac{1}{\Omega_{\mathrm{BZ}}}\int_{\mathrm{BZ}}\underline{\bar{\tau}}(\vec{k})d^{3}k, \tag{2.15}$$

where $\underline{g}(\vec{k})$ is the Fourier transform of $\underline{g}^{nm}$ (the structure constants of the underlying lattice) and Ω_{BZ} is the volume of the BZ. The well-known[24,25] self-consistency condition for determining $\underline{\bar{t}}$ in the KKR-CPA method is now obtained by requiring that the single-site average of $\underline{\tau}^{nn}$ is equal to the corresponding quantity of the effective medium,

$$\langle\underline{\tau}^{nn}\rangle=\langle[\underline{m}^{n}-\underline{\bar{m}}+(\underline{\bar{\tau}}^{nn})^{-1}]^{-1}\rangle=\underline{\bar{\tau}}^{nn}. \tag{2.16}$$

III. CLUSTER METHOD

In this section we derive the cluster generalization of Eq. (2.16). To this end, consider the alloy as a collection of clusters C with corresponding matrix quantities $\underline{\tau}^{CC'}$, $\underline{g}^{CC'}$, and $\underline{t}^{C}$ defined by the relations

$$(\tilde{\tau}^{CC'})^{nm}_{LL'}=\tau^{nm}_{LL'},\quad n\in C,\ m\in C' \tag{3.1a}$$

$$(\tilde{g}^{CC'})^{nm}_{LL'}=g^{nm}_{LL'},\quad n\in C,\ m\in C' \tag{3.1b}$$

and

$$(\tilde{t}^{C})^{nm}_{LL'}=[(\tilde{m}^{C}+\tilde{g}^{C})^{-1}]^{nm}_{LL'},\quad n,m\in C \tag{3.1c}$$

where $\tilde{A}$ denotes a matrix in both site and angular momentum indices. Here, $\tilde{m}^{C}$ is a site-diagonal matrix, $(\tilde{m}^{C})^{nm}_{LL'}=m^{n}_{L}\delta_{nm}\delta_{LL'}$. Quantities analogous to those defined in Eqs. (3.1), corresponding to the effective medium, can also be defined. In particular, the off-diagonal matrix elements $\tilde{\bar{\tau}}^{nm}$ are given by the integrals

$$\underline{\bar{\tau}}^{nm}=\frac{1}{\Omega_{\mathrm{BZ}}}\int\underline{\bar{\tau}}(k)e^{i\vec{k}\cdot\vec{R}_{nm}}d^{3}k. \tag{3.2}$$

With these definitions, the equation of motion of the scattering path operator, Eq. (2.8), can be written in the form

$$\tilde{\tau}^{CC'}=\tilde{t}^{C}\left[\delta_{CC'}+\sum_{C''(\neq C)}\tilde{g}^{CC''}\tilde{\tau}^{C''C'}\right]. \tag{3.3}$$

This equation can be treated formally in a manner analogous to that of Eq. (2.8) and one easily derives the expression

$$\tilde{\tau}^{CC}=[(\tilde{t}^{C})^{-1}-\tilde{\Delta}^{C}]^{-1} \tag{3.4}$$

for the cluster diagonal part of $\tilde{\tau}$. Here, the cluster renormalized interactor $\tilde{\Delta}^{C}$ has site matrix elements

$$(\tilde{\Delta}^{C})^{nm}=\sum_{k\,(\neq C)}\underline{g}^{nk}\underline{m}^{k}\underline{g}^{km}+\sum_{k,l(\neq C)}\underline{g}^{nk}\underline{m}^{k}\underline{g}^{kl}\underline{m}^{l}\underline{g}^{ln}+\cdots , \tag{3.5}$$

where $k\ (\neq C)$ denotes the restriction that k may not assume a value for a site belonging to cluster C. Finally, if the $\underline{m}^{k}$ in Eq. (3.5) are replaced by an effective quantity $\underline{\bar{m}}$, one obtains the equation

$$\tilde{\tau}^{CC}=[\tilde{m}^{C}-\tilde{\bar{m}}^{C}+(\tilde{\bar{\tau}}^{CC})^{-1}]^{-1}, \tag{3.6}$$

in complete analogy with its single-site counterpart, Eq. (2.13). In contrast with the development following Eq. (2.13), no attempt will be made here to determine the quantities $\tilde{\bar{m}}^{C}$ self-consistently with respect to the cluster C. Instead, they will be determined using a simpler self-consistency condition such as the KKR-CPA method. The effects of lack of cluster self-consistency are expected to be small.

Equation (3.6) provides a natural way to treat the effects of local-environment fluctuations within a cluster of real atoms in a substitutionally disordered alloy. Note that the equation yields expressions for any intracluster matrix elements $\underline{\tau}^{nm}$, and hence for $\underline{G}(r,r',\epsilon)$ [see Eq. (2.3)]

for any given cluster configuration. In particular, it yields an expression for the diagonal elements $\underline{\tau}^{nn}$, $n \in C$, which may be used to calculate the site DOS for any site in the cluster. For example, the partial DOS associated with the center of the cluster, site 0, and with any given cluster configuration is given by the expression

$$n_0^{\alpha}(\epsilon) = -\frac{1}{\pi}\mathrm{Im}(\underline{F}^{\alpha})(\bar{\tau}^{CC})_{00} , \tag{3.7}$$

which is a generalization of the formula obtained[24,25] in the KKR-CPA method. Here, all quantities are matrices in angular momentum space; α denotes the occupation of the central site of the cluster, $\alpha = A$ or B, and the matrices F^{α} have matrix elements of the form,

$$F^{\alpha}_{LL'} = \int_{\mathrm{WS}} Z^{\alpha}_{L}(\vec{r}) Z^{\alpha}_{L'}(\vec{r}) d\vec{r} , \tag{3.8}$$

where the integration is over the volume of the Wigner-Seitz (WS) cell. Clearly, Eq. (3.8) can be averaged over cluster configurations and summed to obtain the total DOS associated with the center of the cluster.

IV. CALCULATION OF $\underline{\tau}^{nm}$

It is clear from Eq. (3.6) that an implementation of the cluster method requires the evaluation of all the intracluster matrix elements $\bar{\underline{\tau}}^{nm}$ of the effective-medium scattering path operator. For $l = 2$, each of these elements is a nine-dimensional matrix, which in turn implies that a 13-atom, near-neighbor cluster matrix $\underline{\tau}^{C}$ on an fcc lattice is 117 dimensional. We will describe the method for evaluating $\bar{\underline{\tau}}^{nm}$ and $\underline{\tau}^{nm}$ in some detail.

The rows and columns of the matrix $\bar{\underline{\tau}}(\vec{k})$ can be labeled according to the irreducible representations of the cubic point group. For $l \leq 2$, the relevant representations are Γ_1 (s symmetry), Γ_{15} (p symmetry), $\Gamma_{25'}$ (t_{2g} symmetry), and Γ_{12} (e_g symmetry). Thus the matrix elements of $\bar{\underline{\tau}}(\vec{k})$ can be labeled according to these representations and the corresponding values of l and μ, $\bar{\tau}^{S_1S_2}_{l_1\mu_1,l_2\mu_2}(\vec{k})$, where S_i denotes a particular representation. Equation (3.2) can be written in the form,

$$\bar{\tau}^{S_1S_2}_{l_1\mu_1,l_2\mu_2}(\vec{R}_n) = \frac{1}{\Omega_{\mathrm{BZ}}}\int_{\mathrm{BZ}} \bar{\tau}^{S_1S_2}_{l_1\mu_1,l_2\mu_2}(\vec{k}) e^{i\vec{k}\cdot\vec{R}_n} d^3k = \frac{1}{\Omega_{\mathrm{BZ}}}\sum_{P=1}^{48}\int_{1/48\ \mathrm{BZ}} \bar{\tau}^{S_1S_2}_{l_1\mu_1,l_2\mu_2}(\vec{k}) e^{iP\vec{k}\cdot\vec{R}_n} d^3k , \tag{4.1}$$

where P denotes any one of the 48 symmetry operations of the cubic group, and symmetry has been used to reduce the volume of integration to the irreducible $\frac{1}{48}$ wedge of the Brillouin zone. [For clarity of presentation, we denote $\bar{\underline{\tau}}^{nm}$ by $\bar{\underline{\tau}}(\vec{R}_{nm})$.] The 48 symmetry operations of the cubic group can be divided into two sets, one including 24 operations, and the other including the products of these 24 operations with the inversion operation J. Expression (4.1) can then be written in the form

$$\bar{\tau}^{S_1S_2}_{l_1\mu_1,l_2\mu_2}(\vec{R}_n) = \frac{1}{\Omega_{\mathrm{BZ}}}\sum_{J=0,1}\sum_{P=1}^{24}\int_{1/48\ \mathrm{BZ}} \bar{\tau}^{S_1S_2}_{l_1\mu_1,l_2\mu_2}(JP\vec{k}) e^{iJP\vec{k}\cdot\vec{R}_n} d^3k , \tag{4.2}$$

where the summation over J indicates that the inversion is applied (or not), $J = 1$ (or $J = 0$). Now we can write,

$$\bar{\tau}^{S_1S_2}_{l_1\mu_1,l_2\mu_2}(\vec{R}_n) = \frac{1}{\Omega_{\mathrm{BZ}}}\sum_{P=1}^{24}\int_{1/48\ \mathrm{BZ}} \bar{\tau}^{S_1S_2}_{l_1\mu_1,l_2\mu_2}(P\vec{k})[e^{iP\vec{k}\cdot\vec{R}_n} + (-1)^{l_1-l_2} e^{-iP\vec{k}\cdot\vec{R}_n}] d^3k , \tag{4.3}$$

where use has been made of the fact that

$$\tau^{S_1S_2}_{l_1\mu_1,l_2\mu_2}(\vec{k}) = (-1)^{l_1-l_2}\bar{\tau}^{S_1S_2}_{l_1\mu_1,l_2\mu_2}(-\vec{k}) . \tag{4.4}$$

With the definition

$$E_{l_1l_2}(x) = \begin{cases} 2\cos x & \text{if } l_1 - l_2 \text{ is even,} \\ 2i\sin x & \text{if } l_1 - l_2 \text{ is odd ,} \end{cases} \tag{4.5}$$

we have

$$\bar{\tau}^{S_1S_2}_{l_1\mu_1,l_2\mu_2}(\vec{R}_n) = \frac{1}{\Omega_{\mathrm{BZ}}}\sum_{P=1}^{24}\int_{1/48\ \mathrm{BZ}} \bar{\tau}^{S_1S_2}_{l_1\mu_1,l_2\mu_2}(P\vec{k}) E_{l_1l_2}(P\vec{k}\cdot\vec{R}_n) d^3k . \tag{4.6}$$

Finally, we can use the transformation properties of operators (matrices) under the rotations of the symmetry group to write

$$\bar{\tau}^{S_1S_2}_{l_1\mu_1,l_2\mu_2}(\vec{R}_n) = \frac{1}{\Omega_{\mathrm{BZ}}}\int_{1/48\ \mathrm{BZ}}\left[\sum_{P=1}^{24} D^{S_1}_{l_1\mu_1,l_2\mu_1'}(P)\bar{\tau}^{S_1S_2}_{l_1\mu_1',l_2\mu_2'}(\vec{R})\bar{D}^{S_2}_{l_2\mu_2',l_2\mu_2}(P) E_{l_1,l_2}(\vec{k}\cdot P^{-1}\vec{R}_n)\right]^3 k , \tag{4.7}$$

In this expression, $D^{S}_{l\mu,l'\mu'}(P)$ denotes the $(l\mu,l'\mu')$th element of the matrix representing the operation P in the irreducible representations; $\bar{\underline{D}}$ denotes the transpose of $\underline{D}$, and P^{-1} denotes the inverse of P.

The sum indicated in Eq. (4.7) can be carried out manually or partly programmed on a computer. Owing to symmetry, several of the matrix elements of a given $\bar{\underline{\tau}}(\vec{R}_n)$ are equal to zero. This reduces the number of integrals to be

evaluated numerically and results in substantial savings in computer time.

Having obtained $\bar{\tau}(\vec{R}_n)$ for a particular $\vec{R}_n$, $\bar{\tau}(\vec{R}_m)$ for all $|\vec{R}_m| = |\vec{R}_n|$ is obtained by the transformation

$$\bar{\tau}(\vec{R}_m) = \underline{D}(P_{nm})\bar{\tau}(R_n)\underline{\bar{D}}(P_{nm}) , \tag{4.8}$$

where P_{nm} denotes the rotation operation that takes the vector $\vec{R}_n$ into the vector $\vec{R}_m$. For example, due to inversion symmetry, we have

$$\tau^{S_1S_2}_{l_1\mu_1,l_2\mu_2}(-\vec{R}_n) = \tau^{S_1S_2}_{l_2\mu_2,l_1\mu_1}(\vec{R}_n) . \tag{4.9}$$

Finally, using $\bar{\tau}(\vec{R}_n)$, $\underline{\bar{t}}$, and $\underline{t}$, one obtains $\tilde{\tau}^{nm}$ for any cluster configuration and any energy by inverting the matrix indicated in Eq. (3.6). Explicit expressions for $\bar{\tau}^{nm}$ corresponding to one-dimensional (1D) and three-dimensional (3D) alloys are given in the Appendix.

V. NUMERICAL RESULTS

The cluster method just presented was used to carry out numerical calculations of cluster DOS in model 1D MT alloys as well as in real Ag_cPd_{1-c} alloys.

A. 1D calculations

The 1D alloy of nonoverlapping MT potentials used in our calculations is described by the Hamiltonian

$$H = -\frac{d^2}{dx^2} + \sum_n v(x - na) . \tag{5.1}$$

We assume $v_n(x)$ to be symmetric and to vanish for $|x|$ greater than some radius $S \leq \frac{1}{2}a$, where a is the interatomic spacing. This 1D model retains many of the features of a 3D MT alloy while it presents several computational advantages. Thus in one dimension all BZ integrals can be evaluated analytically, and there exist only two components of the angular momentum, $l=0$ and $l=1$. In addition it is computationally simple to obtain exact DOS histograms using the Schmidt[28] technique and to average over all cluster configurations, at least for small clusters such as near-neighbor clusters. Such averages can be very time consuming for the case of 3D alloys; a near-neighbor cluster of a binary alloy in an fcc lattice gives rise[29] to 288 inequivalent configurations. Thus 1D alloys allow a comparison between exact DOS and those obtained in the KKR-CPA method, as well as in the cluster method.

A detailed description of the application of the KKR-CPA method to 1D MT alloys has been given in previous publications.[30,31] The expressions for the intracluster matrix elements of the scattering path operator for the effective medium $\bar{\tau}^{nm}_{LL'}$ can be calculated analytically and are displayed in the Appendix.

Our calculations were carried out for square-well potentials $v(x)$ of the form shown in Fig. 1, which also shows the band structure of the pure A and B components of the binary alloy A_cB_{1-c}. We present results for the case $c=0.10$. The alloy constituents are defined by the potential parameters as follows: for $v^A(x)$, $V_0^A=-2.0$ and $V_1^A=12.0$, and for $v^B(x)$, $V_0^B=-6.0$ and $V_1^B=2.0$. For both species $x_0=0.4$ and $x_1=0.5$.

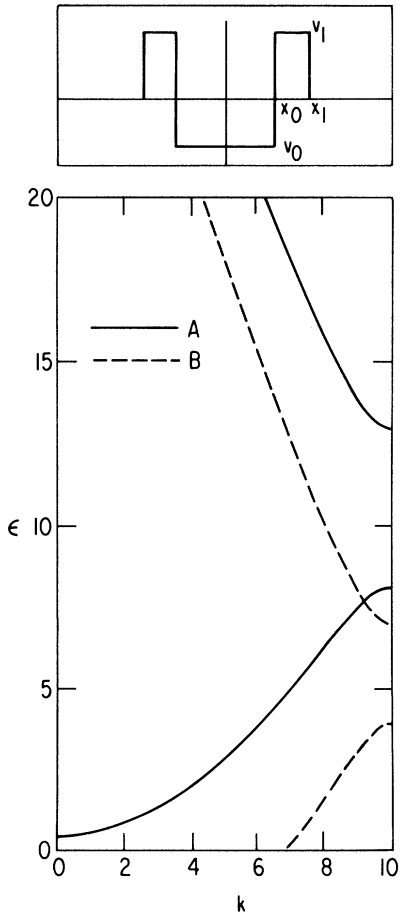

FIG. 1. Upper frame: Schematic of a single $A(B)$ 1D muffin-tin potential. Strength of the potential is defined by the two radii, X_0 and X_1, and by the two constants, V_0 and V_1. Lower frame: Band structure corresponding to an infinite array of A scatterers (solid line) and B scatterers (dashed line); the A and B scatterers are defined by the parameters given in the text.

In the upper frame of Fig. 2 we compare the DOS calculated in the cluster method (solid curve), and in the single-site KKR-CPA method (dashed curve) with an exact DOS histogram. The cluster DOS was calculated for the central site of a three-site cluster and was averaged over all cluster configurations. It can be seen that both the CPA and the cluster DOS agree well with one another and with the exact results; the cluster DOS represents the exact histogram somewhat more faithfully in the high-structure region.

The lower frame in Fig. 2 shows the $l=0$ partial DOS corresponding to an A atom in the KKR-CPA method (dashed curve), and to an A atom surrounded by various configurations of its two near neighbors. When the partial cluster DOS are averaged and combined with the DOS for $l=1$, and with the corresponding DOS for B-centered clusters, they yield the total cluster DOS shown in the upper frame. In the figure, the solid curve corresponds to the configuration BAB, the dotted curve to the configuration BAA, and the dashed-dotted curve to AAA. Such con-

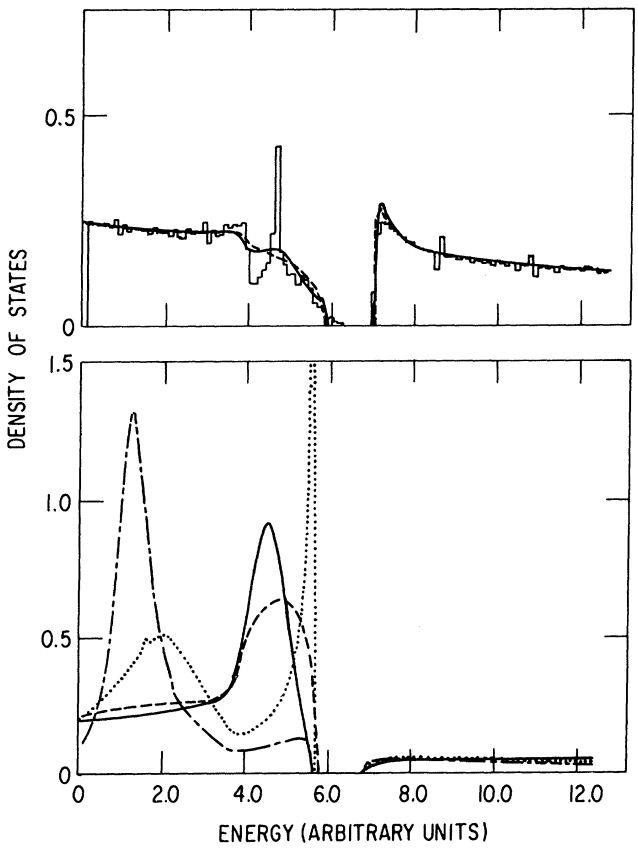

FIG. 2. Upper frame: Total cluster DOS (solid curve) and the KKR-CPA DOS (dashed curve) compared with an exact DOS histogram for the one dimensional alloy $A_{0.10}B_{0.90}$ defined in the text. Lower frame: Component DOS for $l=0$ associated with an atom of type A surrounded by various configurations of its two near neighbors, configuration *BAB* (solid curve), *BAA* (dotted curve), *AAA* (dashed-dotted curve). $l=0$ partial DOS corresponding to an A atom obtained in the KKR-CPA method is also shown (dashed curve).

figurational decompositions pinpoint the origin of much of the structure in the total-DOS curves. For example, it is seen that the high peak in the exact DOS just below the gap originates from configurations of the type *BAB*. We will return to the discussion of the 1D alloy in Sec. V C.

B. Cluster DOS for Ag_cPd_{1-c} alloys

In this subsection we report DOS calculations associated with a near-neighbor cluster of atoms in Ag_cPd_{1-c} alloys. The single-site KKR-CPA method has been implemented[32,33] for Ag_cPd_{1-c} alloys both on the basis of charge non-self-consistent[32] potentials, as well as charge self-consistent[33] alloy potentials within local-density theory. The DOS reported here are associated with the center of a 13-atom nearest-neighbor cluster embedded in a medium determined in the KKR-CPA method for $Ag_{0.5}Pd_{0.5}$ with self-consistent potentials.

Figure 3 shows partial DOS at the center of a near-neighbor cluster for various cluster configurations. The left-four frames show component DOS's for a Ag-centered cluster. Frame (a) shows the s ($l=0$) component DOS for a Ag atom surrounded by (i) 12 Ag atoms (solid curve), (ii) 10 Ag and 2 Pd atoms (dashed-dotted curve), (iii) 6 Ag and 6 Pd atoms (dashed curve), and (iv) 12 Pd atoms (dotted curve). In the configuration containing 10 Ag and 2 Pd atoms, the Pd atoms were second-nearest neighbors of one another, while the 6 Ag and 6 Pd configuration was chosen at random from the many inequivalent configurations possible. It was found that isoatomic configurations, i.e., configurations with equal numbers of atoms of each species, yield quite similar DOS so that classification in terms of numbers of atoms rather than specific configurations is a meaningful approach.

Frame (c) in Fig. 3 show the p component ($l=1$) DOS for the same configurations as those in frame (a), and frame (e) shows the d component ($l=2$) DOS. Frame (g) shows the total DOS at the center of the cluster, i.e., the sum of the DOS shown in frames (a), (c), and (e). Frames (b), (d), (f), and (h) (right column of frames) correspond to frames (a), (c), (e), and (f) but with the roles of Ag and Pd interchanged. Thus the solid curve in frame (b) shows the s-component DOS associated with the center of an all Pd cluster.

The curves depicted in Fig. 3 yield further evidence of the richness in structure that may be displayed by cluster DOS curves as well as of the remarkable regularity in behavior of these curves as functions of cluster content. This reflects the regular behavior of physical properties, and specifically of the DOS, with overall alloy composition found in calculations[32,33] using the KKR-CPA method. Note that the DOS curve for an all-Pd cluster [solid curve in frame (h)] displays the two-peaked structure associated with the bonding (lower peak) and antibonding components of t_{2g} symmetry that is also present in pure Pd DOS. The high, single peak for a Pd atom surrounded by 12 Ag atoms [dotted curve in frame (h)] is the characteristic virtual-level impurity peak observed in DOS calculations[34] of an impurity atom embedded in a pure host, somewhat lowered and broadened by disorder. The DOS curves for intermediate cluster concentrations move gradually from one to the other DOS curves corresponding to these two extreme configurations.

The s- and p- component DOS's (upper-four frames) depend most strongly on the numbers of Ag and Pd atoms in the near-neighbor shell and are almost independent of the occupancy of the central site. For both Ag and Pd atom occupancy of the central site the major peak in the s-component DOS is at about -5.0 eV when the neighbor shell is occupied by 12 Pd atoms, and moves to lower energies with increasing numbers of Ag near neighbors, and ending at about -7.0 eV when all 12 near neighbors are Ag. Presumably the reason for this is that this peak in the s-component DOS on the central site arises from d states situated on the neighboring shell that extend into the central site, and which, when expanded about the central site, contribute to the s-component DOS. Thus this peak is closely tied to the bottom of the d band of the species occuping the neighbor shell, which is lower in energy for Ag than for Pd. This line of reasoning also explains why the internal structure of the s-component DOS near the bottom of the band is closely related to the structure in the

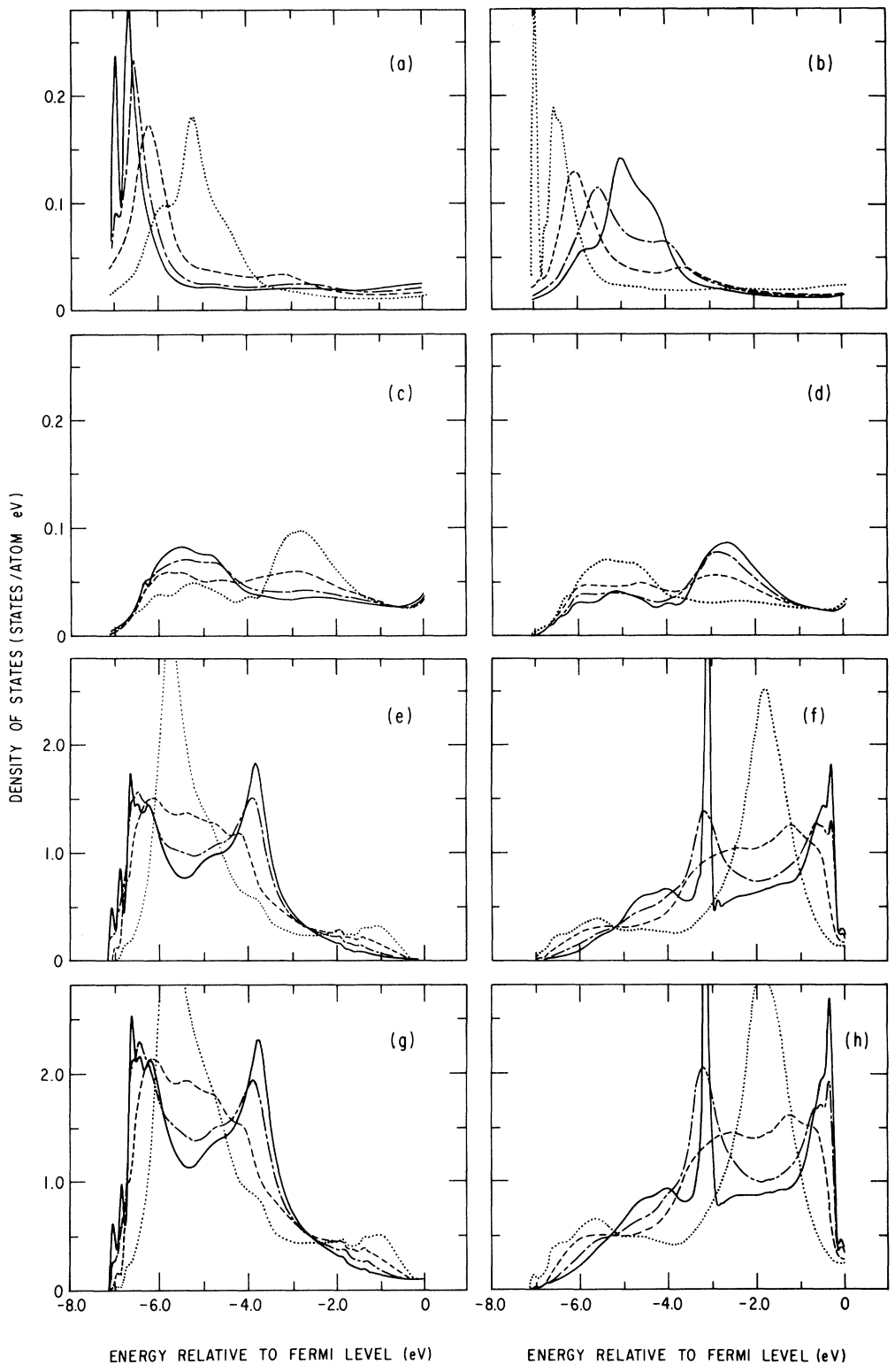

FIG. 3. DOS associated with the center of a near-neighbor cluster in the $Ag_{0.50}Pd_{0.50}$ alloy for various cluster configurations. Ag (Pd) centered cluster DOS are shown on the left (right) column of frames. Frame (a): *s*-component DOS for a Ag atom surrounded by (i) 12 Ag atoms (solid curve), (ii) 10 Ag and 2 Pd atoms (dashed-dotted curve), (iii) 6 Ag and 6 Pd atoms (dashed curve), and (iv) 12 Pd atoms (dotted curve). Frames (c), (e), and (g) depict analogous results for *p*, *d*, and total DOS's, respectively. Frames (b), (d), (f), and (h) show results corresponding to those in frames (a), (c), (e), and (f), but with the roles of Ag and Pd atoms interchanged.

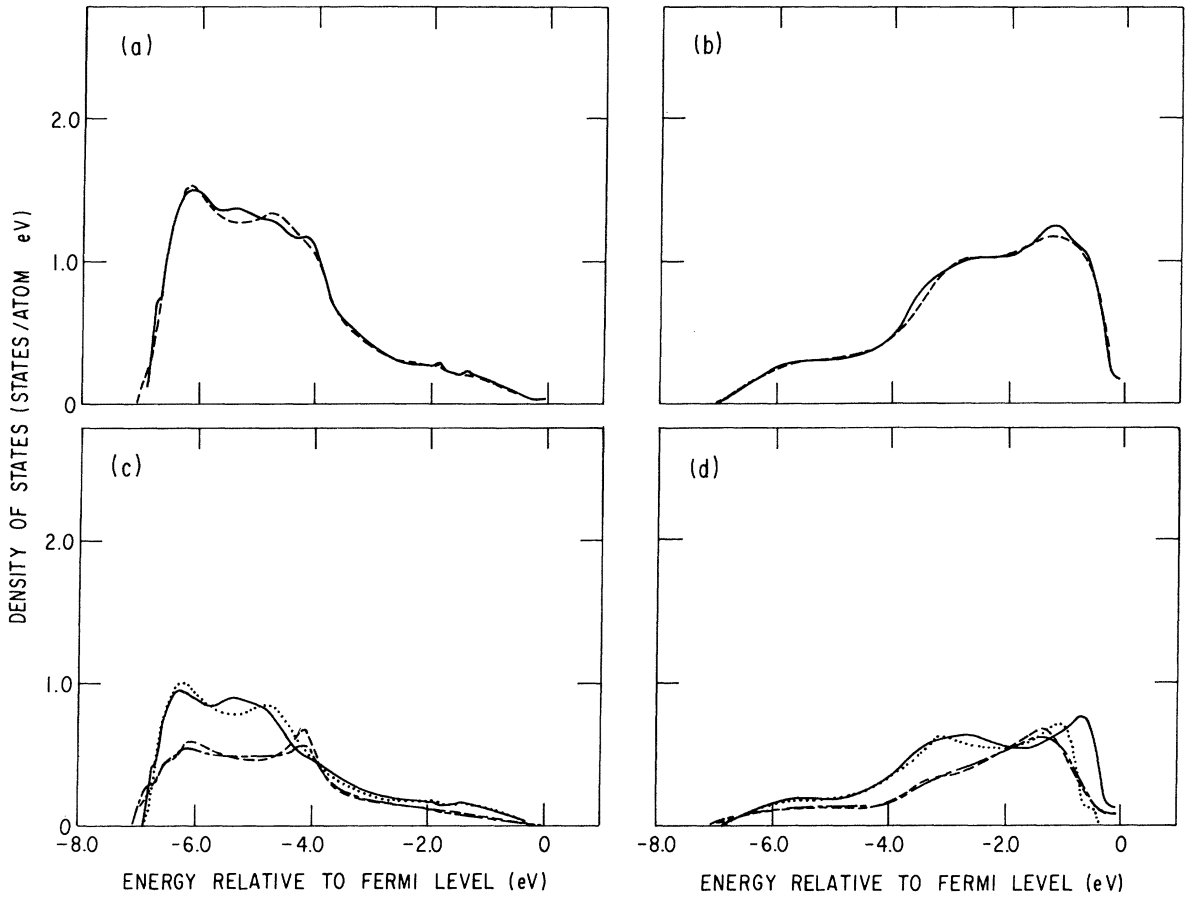

FIG. 4. Frame (a): d-component DOS for a Ag atom surrounded by 6 Ag and 6 Pd atoms (solid curve), compared with the DOS for a Ag atom obtained in the KKR-CPA method (dashed curve). Frame (c): t_{2g}-component DOS (dotted curve) for a Ag atom surrounded by 6 Ag and 6 Pd atoms, and the corresponding DOS obtained in the KKR-CPA method. Corresponding e_g-component DOS's are also shown (dashed-dotted and dashed curves, respectively). Frames (b) and (d) show results analogous to those shown in frames (a) and (c) but with the roles of Ag and Pd atoms interchanged.

d-component DOS in the same energy range. This latter effect is particularly noticeable when all near neighbors are Ag.

Our calculations show that the cluster DOS for cluster (local) concentrations equal (or similar) to the overall alloy concentration are quite similar to the DOS obtained in the single-site KKR-CPA method. This is depicted in frames (a) and (b) of Fig. 4, which show the d-component partial DOS for a Ag and Pd atom each surrounded by 6 Ag and 6 Pd atoms [solid curves in frames (a) and (b), respectively]. The KKR-CPA method DOS's for a Ag and a Pd atom in a 50%-50% Ag-Pd alloy are also shown and are

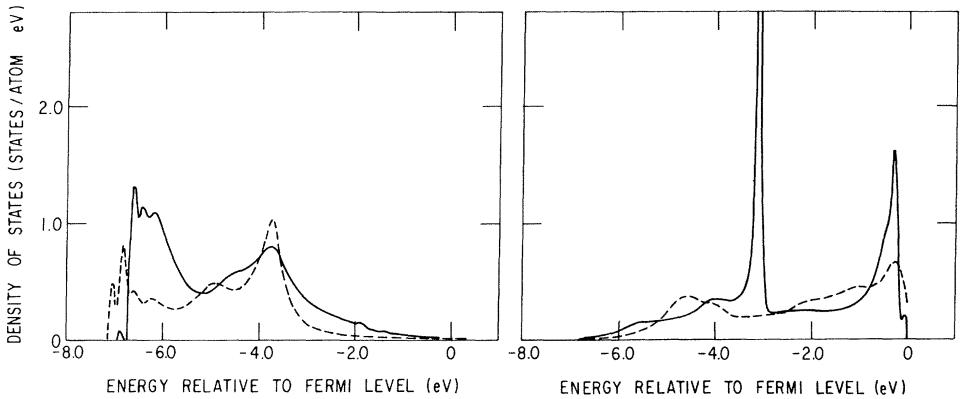

FIG. 5. t_{2g}-component (solid curves) and eg-component (dashed curves) associated with the center of an all-Ag cluster (left frame) and an all-Pd-cluster (right frame).

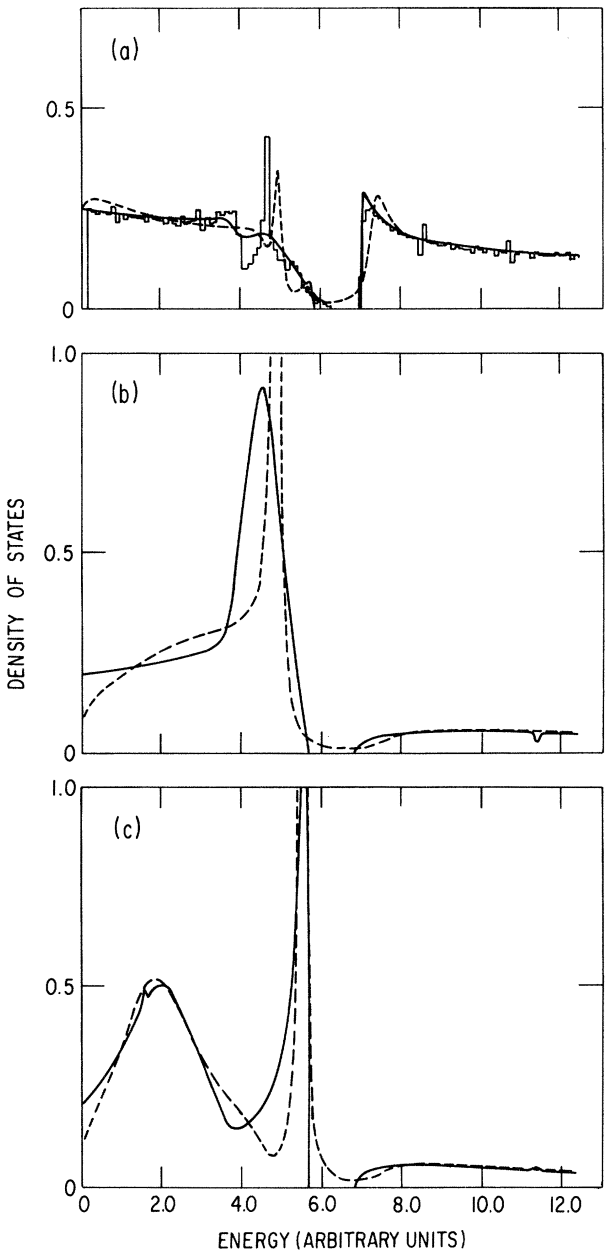

FIG. 6. Frame (a): Total cluster DOS (solid curve) for a three-site cluster embedded in a KKR-CPA medium, and corresponding DOS for a cluster embedded in an ATA medium compared with an exact DOS histogram for the 1D model alloy defined in the text. Frame (b): $l=0$ partial DOS associated with the center of the cluster for the configuration *BAB* for clusters embedded in a KKR-CPA medium (solid curve) and in an ATA medium (dashed curve). Frame (c): Results analogous to those shown in frame (b) but for the configuration *BAA*.

seen to be almost identical to the cluster DOS. The similarity between DOS's corresponding to similar local and overall concentrations persists in the t_{2g}- and e_g-component DOS's. Frames (c) and (d) exhibit the t_{2g}- and e_g-component DOS's obtained in the CPA (dotted and dashed curves, respectively), for a Ag atom [frame (c)] and a Pd atom [frame (d)]. Also shown are the corresponding DOS for a Ag atom surrounded by 6 Ag and 6 Pd atoms (solid and dashed-dotted curves, respectively) in frame (c), and for a Pd atom in frame (d).

Figure 5 depicts the t_{2g} (solid curves) and e_g (dashed curves) components of the d-band DOS at the center of an all Ag cluster (left frame) and an all Pd cluster (right frame). Note that the t_{2g} is much more affected by local fluctuations than the e_g component when compared with the corresponding DOS obtained in the CPA (see Fig. 4, lower frames). This behavior is consistent with the symmetry of the d bands and of an fcc lattice: The t_{2g} component transforms as the functions xy, xz, and yz, which in an fcc lattice are directed along the positions of the nearest neighbors.

C. Clusters embedded in an average—t-matrix approximation medium

Within the context of a single-site approximation, the most serious challenge to the CPA as a viable method for calculating physical properties in substitutionally disordered systems has come from the average—t-matrix approximation[35–37] (ATA). The ATA holds a computational advantage over the CPA since it does not require the solution of self-consistent equations. In the ATA, one approximates the real, disordered alloy by a translationally invariant effective medium characterized by a single-site t matrix that is the weighted average of the t matrices of the alloy constituents. The ATA has been used[36,37] to calculate DOS's in various alloys, and has been compared[30] extensively to the CPA in terms of the 1D model MT Hamiltonian described in Sec. V A. These comparisons firmly establish the CPA as the most satisfactory of the two single-site theories, the computational advantage of the ATA notwithstanding.

It is therefore interesting to inquire as to the possible use of the ATA in connection with a cluster theory. In such an application, one uses Eq. (3.6) to calculate the cluster-diagonal part of the scattering path operator but uses the ATA scattering matrix in the evaluation of the effective-medium quantities $\overline{m}$ and $\overline{\tau}^{nm}$.

Frame (a) in Fig. 6 exhibits DOS curves for the 1D model MT alloy discussed in Sec. V A. Here, the cluster-averaged DOS at the center of a three-site cluster embedded in the CPA, solid curve, and in the ATA, dashed curve, are compared with an exact DOS histogram. It is seen that overall the DOS for the clusters embedded in the CPA represent the exact results somewhat more accurately than do the DOS's for the ATA. Even though there is an attempt by the ATA to reproduce the peak at the low-energy side of the gap, all of the ATA peaks are displaced from the exact results and the ATA curves entirely miss the gap itself. In addition, the ATA curves agree rather poorly with the exact results for energies below the gap. On the other hand, the CPA-embedded cluster DOS's reproduce the gap and follow the rest of the structure of the exact DOS quite faithfully. Previous experience with model TB cluster calculations[38] indicate that self-consistent theories, such as the CPA, produce DOS curves that are smoother as well as more accurate than those pro-

duced by non-self-consistent cluster theories such as the ATA.

Frames (b) and (c) show the $l=0$ DOS's at the center of the cluster for the configurations *BAB* and *BAA*, respectively. It is seen that the CPA-embedded cluster DOS's (solid curves) and their ATA counterparts (dashed curves) agree rather well, while reflecting many of the features of the total DOS shown in the previous figure. Thus the ATA curves are somewhat narrower and displaced with respect to those of the CPA.

Cluster DOS's obtained with CPA- and ATA-embedded clusters are shown in Fig. 7 for the case of the $Ag_{0.5}Pd_{0.5}$ alloy. Here, the solid curve represents the *d*-band DOS at the center of an all-Ag cluster, the dotted curve is the DOS for a Ag atom surrounded by 6 Ag and 6 Pd atoms, and the dashed curve is the Ag-site DOS obtained in the CPA. The dashed-dotted curve is the DOS for a Ag atom surrounded by 6 Ag and 6 Pd atoms embedded in an ATA effective medium. It is seen here that the ATA curve is much more jagged than the CPA curves, especially in the region where the Ag cluster displays a great deal of structure. In a sense, these results are not qualitatively unlike those obtained in the 1D case, since the ATA curves are again found to be less smooth than, and with structure displaced from, the CPA DOS. On the other hand, the differences are much larger, quantitively, in the 3D than in the 1D case. This difference may be partly related to the fact that in three dimensions BZ integrals must be evaluated numerically, whereas analytical expressions are possible in the 1D model. Thus the CPA would seem to provide a medium that yields more reliable numerical results. In any case, further investigation is needed in order to establish the possible usefulness of the ATA in connection with a cluster method such as the one described in this paper.

VI. DISCUSSION

We have presented a method for the calculation of DOS's associated with clusters of atoms in disordered substitutional alloys describable by nonoverlapping MT Hamiltonians. Taken together with similar previous work[22] in connection with TB systems, the method allows the treatment of the effects of local-environment fluctuations in the DOS's in substitutionally disordered systems. This method yields Green's functions and spectral-weight functions having the proper analytic structure, provided that one considers the clusters embedded in an analytic effective medium such as the one determined in the CPA. The method is applicable to multicomponent alloys and allows for the treatment of multiple and/or degenerate bands and of hybridization in a straightforward way.

We have used this method to calculate DOS in both 1D MT model alloys and in Ag_cPd_{1-c} alloys. Our numerical results show that the effects on the central-site DOS's of fluctuations in the chemical occupation of the first shell can be large. These results also show a regular variation of the DOS as a function of local environment, which can be understood in terms of basic notions such as the symmetry of the lattice and the relative scattering strengths of the alloy constituents. Finally, even though the effects of fluctuations in coordination shells beyond the first must

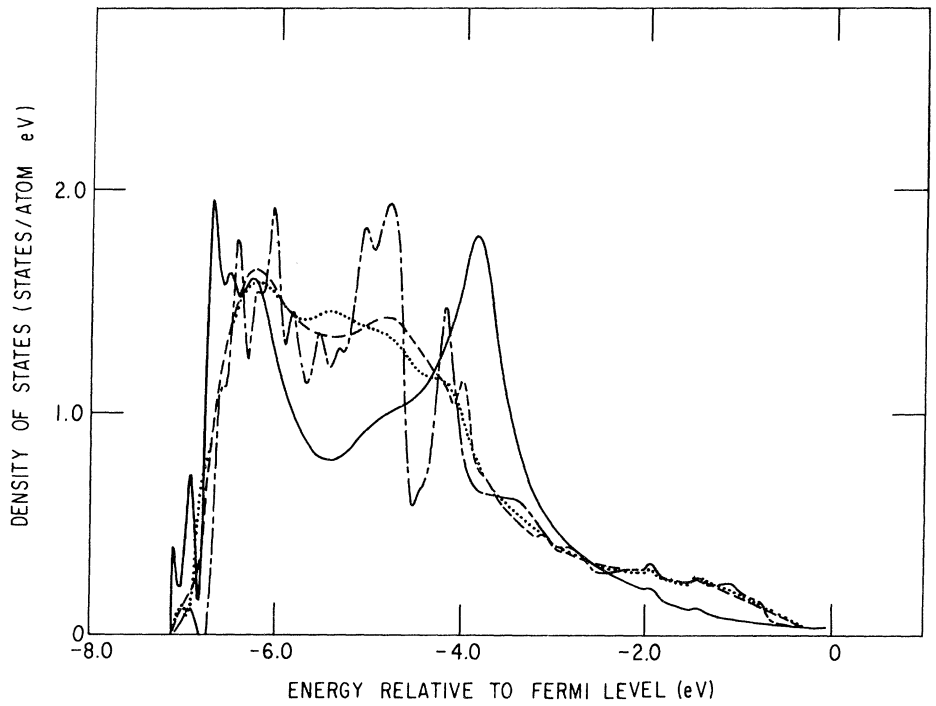

FIG. 7. DOS associated with the center of near-neighbor clusters embedded in a KKR-CPA and an ATA effective-medium. *d*-band DOS for a Ag atom surrounded by (i) 12 Ag atoms embedded in KKR-CPA medium (solid curve), (ii) 6 Ag and 6 Pd atoms embedded in a KKR-CPA medium, (iii) 6 Ag and 6 Pd atoms embedded in an ATA medium (dashed-dotted curve), and for a Ag atom in the KKR-CPA method (dashed curve).

be of some importance, these effects die out rapidly with increasing shell number for realistic 2D and 3D systems. For such systems, we anticipate that calculations such as those presented in this paper will suffice for the determination of many physical observables in disordered systems.

The detailed information provided by cluster calculations of the type reported in this paper affords one a great freedom in the investigation of the physical properties of disordered systems. One possible and immediate application is related to the questions of charge transfer and SRO in substitutionally disordered alloys. Such an application has been undertaken and initial results are being reported[39] elsewhere. Further applications can be made in connection with magnetic moment formation and the transport properties of disordered systems.

Investigations of this sort as well as further experience with other alloy systems are being prepared. Also, attempts will be made to carry the cluster calculations to electronic self-consistency within local-density theory. Such a task is indeed computationally difficult but may be realistic at least for cluster configurations with rotational symmetry.

ACKNOWLEDGMENTS

The authors wish to thank J. S. Faulkner for many stimulating discussions, insights, and moral support during the completion of the project. One of the authors (A.G.) is grateful to J. W. Garland for useful conversations and thanks N. K. Flevaris for helpful comments. He is also indebted to the Metals and Ceramics Division of the Oak Ridge National Laboratory for the financial support that made much of this work possible. This research was sponsored by the Division of Materials Sciences, U.S. Department of Energy, under Contract No. W-7405-eng-26 with the Union Carbide Corporation.

APPENDIX

In order to exemplify the formalism presented in the main body of the paper, we present explicit expressions for various matrix elements of the cluster matrix $\bar{\bar{\tau}}^{CC}$, for both (1D) and (3D) systems.

1. 1D Systems

The KKR formalism for determining the band structure of pure 1D materials, as well as the formalism for the KKR-CPA method for such materials, has been described fully by Butler.[31] In a previous publication[30] extensive calculations based on that formalism and using the 1D model MT alloy potentials described in Sec. V were reported.

The point group of a 1D lattice contains only the identity and the inversion operations. Thus 1D systems are characterized by only two values of l, $l=0$ and $l=1$, corresponding to even and odd parity. Letting δ_l^α denote the phase shift for a given value of l corresponding to the potential for species α, we have

$$t_l^\alpha = -\sqrt{E}\, e^{i\delta_l^\alpha} \sin\delta_l^\alpha \ . \tag{A1}$$

The effective scattering matrices $\bar{t}_l$ determined in the KKR-CPA method can be expressed in terms of effective (in general complex) phase shifts δ_l. By defining the quantities

$$x = \cos(\phi+\delta_0+\delta_1)/\cos(\delta_0-\delta_1) \ , \tag{A2a}$$

$$f_0 = \cos\phi - \tan\delta_0 \sin\phi \ , \tag{A2b}$$

$$f_1 = \cos\phi - \tan\delta_1 \sin\phi \ , \tag{A2c}$$

and

$$I(x,f) = 1 + (x-f)/(x^2-1)^{1/2} \ , \tag{A2d}$$

where ϕ is $\sqrt{E}$ times the lattice constant a, it can be shown[31] that the matrix elements $\bar{\tau}_{00}^{00}$ and $\bar{\tau}_{11}^{00}$ (the scattering path operator for site 0 and $l=0$ and 1) are given by the expressions,

$$\bar{\tau}_{00}^{00} = -\sqrt{E}\,\frac{\tan\delta_0}{1+\tan\delta_0\tan\delta_1} I(x,f_1) = 2\pi\alpha I(x,f_1) \tag{A3a}$$

$$\bar{\tau}_{00}^{00} = -\sqrt{E}\,\frac{\tan\delta_1}{1+\tan\delta_0\tan\delta_1} I(x,f_0) = 2\pi\beta I(x,f_0) \ , \tag{A3b}$$

and

$$\bar{\tau}_{01}^{00} = \bar{\tau}_{10}^{00} = 0 \ . \tag{A3c}$$

The last expression, Eq. (A3c), is a consequence of the odd parity of $\bar{\tau}(\vec{k})$, which implies that $\bar{\tau}_{10}^{00} = -\bar{\tau}_{10}^{00} = 0$.

Now consider a cluster of three sites, labeled consecutively $\bar{1}$, 0, and 1, embedded in a KKR-CPA effective medium. The effective-medium cluster matrix $\bar{\bar{\tau}}^{CC}$ can be written in the form

$$\bar{\bar{\tau}}^{CC} = \begin{bmatrix} \bar{\tau}^{00} & \bar{\tau}^{01} & \bar{\tau}^{0\bar{1}} \\ \bar{\tau}^{10} & \bar{\tau}^{11} & \bar{\tau}^{1\bar{1}} \\ \bar{\tau}^{\bar{1}0} & \bar{\tau}^{\bar{1}1} & \bar{\tau}^{\bar{1}\bar{1}} \end{bmatrix} \ , \tag{A4}$$

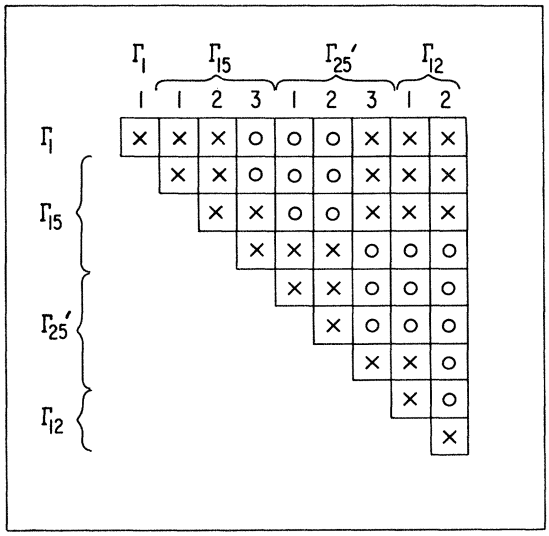

FIG. 8. Structure of the 9×9 matrix for the near-neighbor matrix element $\bar{\tau}^{nm}$ with $\vec{R}_{nm} = \vec{R}_{(110)}$.

where each matrix element $\underline{\tau}^{ij}$ is a 2×2 matrix in l space. In particular,

$$\underline{\tau}^{00}=\underline{\tau}^{11}=\begin{bmatrix}\bar{\tau}_{00}^{00} & 0\\ 0 & \bar{\tau}_{11}^{00}\end{bmatrix}, \tag{A5}$$

where $\bar{\tau}_{00}^{00}$ and $\bar{\tau}_{11}^{00}$ are given by Eqs. (A3). The other elements of $\bar{\bar{\tau}}^{CC}$ can be evaluated analytically by performing the integrations indicated in Eq. (4.1), which for 1D systems reduce to contour integrals over the unit circle. With $\gamma=\alpha\tan\delta_1=\beta\tan\delta_0$, we find

$$\underline{\tau}^{01}=\begin{bmatrix}(-\alpha f_1+x\bar{\tau}_{00}^{00}) & -\gamma[x+(1-x^2)/(x^2-1)^{1/2}]\\ \gamma[x+(1-x^2)/(x^2-1)^{1/2}] & (-\beta f_0+x\bar{\tau}_{11}^{00})\end{bmatrix} \tag{A6}$$

and

$$\underline{\tau}^{1\bar{1}}=\begin{bmatrix}[\alpha-\bar{\tau}_{00}^{00}+2x\bar{\tau}_{00}^{01}] & -\gamma[1-2x^2-2x(x^2-1)^{1/2}]\\ \gamma[1-2x^2-2x(x^2-1)^{1/2}] & (\beta-\bar{\tau}_{11}^{00}+2x\bar{\tau}_{11}^{01})\end{bmatrix}. \tag{A7}$$

Equations (A3) and (A5)–(A7) along with relations $(\underline{\tau}^{CC})_{\mu\nu}=(\underline{\tau}^{CC})_{\nu\mu}$ completely determine $\bar{\bar{\tau}}^{CC}$.

2. 3D Systems

For 3D systems, the integrals in Eq. (3.1) [or equivalently in Eq. (4.1)] must be evaluated numerically. The integrations were carried out over the irreducible $\frac{1}{48}$th of the BZ as is indicated in Eq. (4.7), using the ray technique that has been described elsewhere.[3] In the following expressions, we use a notation where $\vec{k}$ stands for $(a/2)\vec{k}$, and we identify the matrix elements of $\underline{\tau}(\vec{k})$ with the l,μ indices, neglecting the symmetry superscripts S for the sake of clarity.

For $\vec{R}_n=0$, $\underline{\tau}(0)$ is diagonal and its matrix elements are given by the integrals of the expressions

$$[\bar{\tau}(0)]_{11}=[\bar{\tau}(0)]_{00,00}^{\Gamma_1\Gamma_1}=\frac{48}{\Omega_{BZ}}\int_{1/48\ BZ}d^3k[\bar{\tau}(\vec{k})_{00,00}], \tag{A8a}$$

$$\begin{aligned}[\tau(0)]_{22}&=[\bar{\tau}(0)]_{1\bar{1},1\bar{1}}^{\Gamma_{15}\Gamma_{15}}\\ &=\frac{16}{\Omega_{BZ}}\int_{1/48\ BZ}d^3k[\bar{\tau}(\vec{k})_{1\bar{1},1\bar{1}}+\bar{\tau}(\vec{k})_{10,10}\\ &\qquad+\bar{\tau}(\vec{k})_{11,11}]\\ &=\bar{\tau}(0)_{33}\\ &=\bar{\tau}(0)_{44},\end{aligned} \tag{A8b}$$

$$\begin{aligned}[\bar{\tau}(0)]_{55}&=[\bar{\tau}(0)]_{2\bar{2},2\bar{2}}^{\Gamma_{25'}\Gamma_{25'}}\\ &=\frac{16}{\Omega_{BZ}}\int_{1/48\ BZ}d^3k[\bar{\tau}(\vec{k})_{2\bar{2},2\bar{2}}+\bar{\tau}(\vec{k})_{2\bar{1},2\bar{1}}\\ &\qquad+\bar{\tau}(\vec{k})_{21,21}]\\ &=\bar{\tau}(0)_{66}\\ &=\bar{\tau}(0)_{88},\end{aligned} \tag{A8c}$$

and

$$\begin{aligned}[\bar{\tau}(0)]_{77}&=[\bar{\tau}(0)]_{20,20}^{\Gamma_{12}\Gamma_{12}}\\ &=\frac{24}{\Omega_{BZ}}\int_{1/48\ BZ}d^3k[\bar{\tau}(\vec{k})_{20,20}+\bar{\tau}(\vec{k})_{22,22}]\\ &=\bar{\tau}(0)_{99}.\end{aligned} \tag{A8d}$$

For $\vec{R}_n=\vec{R}_{110}$, there are 17 nonvanishing matrix elements of $\underline{\tau}(\vec{R}_{110})$, as is indicated by the $\times$'s in Fig. 8. These elements are obtained as the integrals of expressions such as those shown below:

$$[\bar{\tau}(\vec{R}_{110})]_{11}=[\bar{\tau}(\vec{R}_{110})]_{00,00}^{\Gamma_1\Gamma_1}=\frac{16}{\Omega_{BZ}}\int_{1/48\ BZ}d^3k[(\cos k_x\cos k_y+\cos k_y\cos k_z+\cos k_x\cos k_z)\bar{\tau}(\vec{k})_{00,00}], \tag{A9a}$$

$$\begin{aligned}[\bar{\tau}(\vec{R}_{110})]_{29}&=[\bar{\tau}(\vec{R}_{110})]_{1\bar{1},22}^{\Gamma_{15}\Gamma_{12}}\\ &=\frac{4}{\Omega_{BZ}}\int_{1/48\ BZ}d^3k[-\sqrt{3}\sin k_x\cos k_z\bar{\tau}(\vec{k})_{11,21}+\sin k_x(2\cos k_y+\cos k_z)\bar{\tau}(\vec{k})_{11,22}\\ &\qquad-\sqrt{3}\sin k_y\cos k_z\bar{\tau}(\vec{k})_{1\bar{1},20}-\sin k_y(2\cos k_x+\cos k_z)\bar{\tau}(\vec{k})_{1\bar{1},22}\\ &\qquad+\sqrt{3}\sin k_z(\cos k_x+\cos k_y)\bar{\tau}(\vec{k})_{10,20}+\sin k_z(\cos k_y-\cos k_x)\bar{\tau}(\vec{k})_{10,22}].\end{aligned} \tag{A9b}$$

For a near-neighbor cluster in an fcc lattice, there are 82 such complex integrals to be evaluated numerically corresponding to intracluster vectors $\vec{R}_{000}$, $\vec{R}_{110}$, $\vec{R}_{200}$, $\vec{R}_{211}$, and $\vec{R}_{220}$. The other $\underline{\tau}(\vec{R}_n)$ can be obtained by the use of Eq. (4.8).

[1]P. Soven, Phys. Rev. 156, 809 (1967).
[2]R. J. Elliott, J. A. Krumhansl, and P. L. Leath, Rev. Mod. Phys. 46, 465 (1974).
[3]B. L. Gyorffy and G. M. Stocks, in *Electrons in Disordered Metals and Metallic Surfaces,* edited by P. Phariseau, B. L. Gyorffy, and L. Scheire (Plenum, New York, 1978), p. 89, and references therein.
[4]B. Velicky, S. Kirkpatrick, and H. Ehrenreich, Phys. Rev. 175, 747 (1968).
[5]G. M. Stocks, R. W. Williams, and J. S. Faulkner, Phys. Rev. B 4, 4390 (1971); J. Phys. F 3, 1688 (1973).
[6]B. Velicky, Phys. Rev. 184, 614 (1969).
[7]T. Kaplan, P. L. Leath, L. J. Gray, and H. W. Diehl, Phys. Rev. B 21, 4230 (1980).
[8]R. Mills and P. Ratanavararaksa, Phys. Rev. B 18, 5291 (1978).
[9]N. Zaman and R. J. Jacobs, J. Phys. F 5, 1677 (1975).
[10]K. Aoi, Solid State Commun. 14, 929 (1974).
[11]F. Brouers, M. Cyrot, and F. Cyrot-Lackmann, Phys. Rev. B 7, 4370 (1973).
[12]F. Brouers, F. Ducastelle, and J. Van der Rest, J. Phys. F 3, 1704 (1973).
[13]F. Brouers and F. Ducastelle, J. Phys. F 5, 45 (1975).
[14]T. Miwa, Prog. Theor. Phys. 52, 1 (1974).
[15]N. F. Berk and R. A. Tahir-Kheli, Physica 67, 501 (1973).
[16]N. F. Berk, J. Shazeer, and R. A. Tahir-Kheli, Phys. Rev. B 8, 2496 (1973).
[17]A. R. Bishop and A. Mookerjee, J. Phys. C 7, 2165 (1973).
[18]P. Lloyd and P. R. Best, J. Phys. C 8, 3752 (1975).
[19]M. Tsukada, J. Phys. Soc. Jpn. 32, 1475 (1972).
[20]B. G. Nickel and W. H. Butler, Phys. Rev. Lett. 30, 373 (1972).
[21]F. Cyrot-Lackmann and M. Cyrot, Solid State Commun. 22, 517 (1977).
[22]A. Gonis and J. W. Garland, Phys. Rev. B 16, 2424 (1977).
[23]Charles W. Myles and John D. Dow, Phys. Rev. Lett. 42, 254 (1979); Phys. Rev. B 19, 4939 (1979).
[24]J. S. Faulkner and G. M. Stocks, Phys. Rev. B 21, 3222 (1980).
[25]J. S. Faulkner, in *Progress in Material Science,* edited by J. W. Christian, P. Hassen, and T. B. Massalski (Pergammon, New York, 1982), Vols. 1 and 2.
[26]B. L. Gyorffy and M. J. Stott, in *Band Structure Spectroscopy of Metals and Alloys,* edited by D. J. Fabian and L. M. Watson (Academic, New York, 1973), pp. 385.
[27]W. M. Temmerman, J. Phys. F 12, L25 (1982).
[28]H. Schmidt, Phys. Rev. 105, 425 (1957).
[29]P. C. Clapp, Ledgemont Laboratory (Kennecott Copper Corporation, Lexington, Massachusetts 02173) Technical Report No. 249, 1970 (unpublished).
[30]A. Gonis and G. M. Stocks, Phys. Rev. B 25, 659 (1982).
[31]W. H. Butler, Phys. Rev. B 14, 468 (1976).
[32]A. J. Pindor, W. M. Temmerman, B. L. Gyorffy, and G. M. Stocks, J. Phys. F 10, 2617 (1980).
[33]H. Winter and G. M. Stocks, Phys. Rev. B 27, 882 (1983).
[34]R. Podloucky, R. Zeller, and P. H. Dederichs, Phys. Rev. B 22, 5777 (1980).
[35]J. Korringa, J. Phys. Chem. Solids 7, 252 (1958).
[36]L. Schwartz and A. Bansil, Phys. Rev. B 10, 3261 (1979).
[37]A. Bansil, Phys. Rev. B 10, 4025 (1979); 10, 4035 (1979).
[38]A. Gonis (unpublished).
[39]A. Gonis, W. H. Butler, and G. M. Stocks, Phys. Rev. Lett. 50, 1482 (1983).